A Novel Approach for Spectral Unmixing, Classification, and Concentration Estimation of Chemical and Biological Agents

Chiman Kwan, *Senior Member, IEEE*, Bulent Ayhan, *Student Member, IEEE*, Genshe Chen, *Member, IEEE*, Jing Wang, Baohong Ji, *Student Member, IEEE*, and Chein-I Chang, *Senior Member, IEEE*

Abstract—In this paper, spectral unmixing methods, which are extensively used in hyperspectral imaging area, are proposed for classification and abundance fraction (concentration) estimation of chemical and biological agents that exist in the mixture form. Several government-furnished datasets, which were collected through the infrared spectrum method, were thoroughly analyzed. Two similarity measures—the spectral angle mapper and spectral information divergence—were investigated in order to provide a quantitative comparison basis with respect to the performance of the applied spectral unmixing methods in the existence of similar and distinct agents. The use of the similarity measures provided valuable information about the signature characteristics of the agents, which led to a better understanding about the capabilities of the investigated methods. The orthogonal subspace projection (OSP) method was investigated as the first unmixing, classification, and abundance estimation technique. It was observed that the OSP method provided good results when the number of agents in the database was small and was composed of distinct agents. However, when the number of agents was incremented by adding agents that share similar characteristics, the abundance estimation accuracy gradually degraded in addition to generating negative abundance fraction estimates. The second investigated unmixing method was called nonnegatively constrained least squares (NCLS). The results and analyses indicated that the NCLS method outperformed the OSP approach by providing considerably more accurate fraction estimates while at the same time not generating any negative fraction estimates; thus, the use of the NCLS method was found to be promising in detection and abundance fraction estimation of chemical and biological agents that exist in the form of mixtures. In addition, efficient implementation of NCLS has resulted in much lower computations than the conventional OSP implementation.

Index Terms—Biological agent detection, chemical agent detection, nonnegatively constrained least squares (NCLS), orthogonal subspace projection (OSP).

I. INTRODUCTION

CHEMICAL and biological defense are important for both military and civilian applications. The capability to quickly detect and classify different chemical and biological agents (CBAs) will provide ample time for soldiers and law enforcement personnel to prepare and counteract these agents. This issue has become more and more important after September 11, 2001. Terrorist attacks by using chemical and biological agents to cities in the U.S. are no longer remote possibilities now. Early detection of CBAs may give an indication of terrorist activity that may allow proper procedures to be followed to mitigate dangers and protect civilians in public places and also military personnel patrolling areas that are risky for terrorist attacks.

There are several chemical and biological agent detection techniques which are in use or under study [1]. These techniques can be considered as feature extraction methods that transform chemical and biological quantities into characteristic signatures. The use of surface acoustic wave sensors (SAWS) is one of these techniques. Surface acoustic wave sensors are devices that measure the mass of materials that stick to the surface of the sensor [2]. The selectivity of the sensor depends on the selectivity of the coating, where organic polymers are generally used as coatings in chemical agent detection [2]. Ion mobility spectrometry is another technique. This technique is based on the fact that ionization of analytes in air produces electric current when they collide with a detector plate [3]. Gas chromatography (GC) and mass spectrometry (MS) are two other well-known techniques in this field. Microwave spectroscopy is another technique, which is noted to have the quantitative power of GC/MS methods, with some additional benefits such as significantly reducing the false positive detection rate and improving the analysis time [4]. Finally, there are the spectroscopic techniques such as the Fourier transform infrared spectrum (FT-IR), which are noted to have higher information content than other agent detection techniques [2]. However, a fast scanning instrument together with a fast computer is required in order to do continuous monitoring and process all the available information in a short period of time.

In a chemical and biological agent attack, it is possible that the chemical and biological agents can be composed in the form of mixtures in order to make the existing agent detection systems, which are specific to single agents, useless. The detection of agents in the form of mixtures is a more challenging problem than detecting the agents alone. The accurate and robust detection of such chemical or biological agent concentrations is a major key to success. One approach is to find unique spectral attributes that are indicative of the chemical agents that form the mixture [2]. When the agents are mixed, the resultant agent mixture signature differs from the agent signatures that are components of the mixture, and depends on the abundance fractions of the components. It becomes a difficult problem to come up with a pattern recognition type of detection system since the number of cases

C. Kwan, B. Ayhan, and G. Chen are with Intelligent Automation, Inc., Rockville, MD 20855 USA (e-mail: ckwan@i-a-i.com).

J. Wang, B. Ji, and C.-I Chang are with the Department of Computer Science and Electrical Engineering, Remote Sensing Signal and Image Processing Laboratory, University of Maryland Baltimore County, Baltimore, MD 21250 USA.

for forming agent mixtures is endless. Thus, generating a database that consists of every possible agent mixture combination is not practical. Instead of a pattern recognition type of detection system, a spectral unmixing algorithm, which has the capability of decomposing the agents in the mixture and estimating their abundance fractions in the mixture, has to be carried out in an effective manner.

In the last decade, many useful methods such as orthogonal subspace projection (OSP), nonnegatively constrained least squares (NCLS), etc., have been developed in the area of multispectral/hyperspectral image analysis [5]–[10]. Application of these algorithms to two-dimensional images significantly improved the target detection and identification performance. The focus of this research was to apply some of the new techniques in multispectral/hyperspectral area to detect, classify, and estimate concentration of CBAs in mixtures of chemical and biological agents. The datasets used in this work were provided by the National Institute of Standards and Technology (NIST) and the U.S. Army. These datasets contained the signatures of the chemical and biological agents of interest. These signatures were obtained experimentally by the infrared (IR) spectrum technique. In order to investigate the detection and abundance fraction estimation performance of the applied spectral unmixing methods, agent mixtures were formed. In forming these mixtures a linear mixing methodology was conducted. First, the selected agents that form the mixture were multiplied with some fraction values which have values greater than 0. Afterward, these were summed to form the resultant agent mixture signature.

Two spectral metrics—the spectral angle mapper (SAM) and spectral information divergence (SID)—were investigated in order to assess the similarity of the agents. This assessment was needed to explain why some agents are difficult to classify and how the applied spectral unmixing methods perform in the existence of similar and distinct agents. Two spectral unmixing methods have been investigated: OSP and NCLS [5], [6]. It was observed that OSP performs well when noise level was low and the number of agents in the mixture was small. However, the performance of OSP dropped significantly when the noise level was high and the number of agents was large. Moreover, in the concentration estimation part, negative concentration estimates showed up, which was highly undesirable. OSP cannot effectively deal with agents with similar spectral characteristics. In contrast, NCLS achieved accurate results in noisy conditions, in the presence of similar agents, and with a large number of agents in a mixture (up to 20 agents in our studies). Efficient implementation of NCLS achieved near real-time performance. Thus, the NCLS method was found to be promising in detecting chemical and biological agents, which are in the form of mixtures. In addition to correct detection of the agents, the abundance fractions of the detected agents were estimated accurately with the NCLS method.

This paper is organized as follows. Section II summarizes the algorithms studied in this research. Details of the SAM and SID similarity measures and the two investigated spectral unmixing algorithms OSP and NCLS are described in this section. Section III describes the conducted experiments and the corresponding analyses for the experiments. Finally, conclusions are drawn in Section IV.

II. ALGORITHMS

The key technical approach in the conducted analysis and experiments is based on two spectral unmixing and abundance fraction estimation techniques: the orthogonal subspace projection and the nonnegatively constrained least squares methods [5]. Two similarity measures have been investigated as well in applying these unmixing techniques to various government-furnished datasets: the spectral angle mapper and the spectral information divergence methods. First, the two similarity measures SAM and SID are introduced. Following that the two unmixing methods OSP and NCLS are described in this section.

A. Similarity Measures

1) SAM: Assume that $\mathbf{s}_i = (s_{i1}, s_{i2}, \ldots, s_{iL})^T$ and $\mathbf{s}_j = (s_{j1}, s_{j2}, \ldots, s_{jL})^T$ are two spectral signatures. The SAM measures spectral similarity by finding the angle between the spectral signatures $\boldsymbol{s}_i$ and $\boldsymbol{s}_j$

$$\mathrm{SAM}(\mathbf{s}_i, \mathbf{s}_j) = \cos^{-1}\left(\frac{\langle \mathbf{s}_i, \mathbf{s}_j \rangle}{\|\mathbf{s}_i\| \|\mathbf{s}_j\|}\right) \quad (1)$$

where $\langle \mathbf{s}_i, \mathbf{s}_j \rangle = \sum_{l=1}^{L} s_{il} s_{jl}$, $\|\mathbf{s}_i\| = \left(\sum_{l=1}^{L} s_{il}^2\right)^{1/2}$, and $\|\mathbf{s}_j\| = \left(\sum_{l=1}^{L} (s_{jl})^2\right)^{1/2}$.

2) SID: Let $\mathbf{p} = (p_1, p_2, \ldots, p_L)^T$ and $\mathbf{q} = (q_1, q_2, \ldots, q_L)^T$ be the two probability mass functions generated by $\mathbf{s}_i = (s_{i1}, s_{i2}, \ldots, s_{iL})^T$ and $\mathbf{s}_j = (s_{j1}, s_{j2}, \ldots, s_{jL})^T$, respectively, with $p_l = s_{il}/\sum_{l=1}^{L} s_{il}$ and $q_l = s_{jl}/\sum_{l=1}^{L} s_{jl}$. So, the self-information provided by $\boldsymbol{s}_i$ and $\boldsymbol{s}_j$ for band l is defined by

$$I_l(\mathbf{s}_i) = -\log p_l \quad (2)$$
$$I_l(\mathbf{s}_j) = -\log q_l. \quad (3)$$

By virtue of (2) and (3), the discrepancy of the self-information of band image B_l provided by $\mathbf{s}_j$ relative to the self-information of band image B_l provided by $\mathbf{s}_i$, denoted by $D_l(\mathbf{s}_i \,\|\, \mathbf{s}_j)$, can be defined as

$$D_l(\mathbf{s}_i \,\|\, \mathbf{s}_j) = I_l(\mathbf{s}_j) - I_l(\mathbf{s}_i) = \log\left(\frac{p_l}{q_l}\right). \quad (4)$$

Averaging $D_l(\mathbf{s}_i \,\|\, \mathbf{s}_j)$ in (4) over all the bands $\{B_l\}_{l=1}^{L}$ results in

$$D(\mathbf{s}_i \,\|\, \mathbf{s}_j) = \sum_{l=1}^{L} D_l(\mathbf{s}_i \,\|\, \mathbf{s}_j) p_l = \sum_{l=1}^{L} p_l \log\left(\frac{p_l}{q_l}\right) \quad (5)$$

where $D(\mathbf{s}_i \,\|\, \mathbf{s}_j)$ is the average discrepancy in the self-information of $\mathbf{s}_j$ relative to the self-information of $\mathbf{s}_i$. In the context of information theory, $D(\mathbf{s}_i \,\|\, \mathbf{s}_j)$ in (5) is called the relative entropy of $\mathbf{s}_j$ with respect to $\mathbf{s}_i$ which is also known as the Kullback–Leibler information measure, directed divergence or cross entropy [11]. Similarly, the average discrepancy in the self-information of $\mathbf{s}_i$ relative to the self-information of $\mathbf{s}_j$ can be defined by

$$D(\mathbf{s}_j \,\|\, \mathbf{s}_i) = \sum_{l=1}^{L} D_l(\mathbf{s}_j \,\|\, \mathbf{s}_i) q_l = \sum_{l=1}^{L} q_l \log\left(\frac{q_l}{p_l}\right). \quad (6)$$

Summing (5) and (6) yields SID defined by

$$\mathrm{SID}(\mathbf{s}_i, \mathbf{s}_j) = D(\mathbf{s}_i \,\|\, \mathbf{s}_j) + D(\mathbf{s}_j \,\|\, \mathbf{s}_i) \quad (7)$$

which can be used to measure the discrepancy between two pixel vectors $\mathbf{s}_i$ and $\mathbf{s}_j$ in terms of their corresponding probability mass functions, $\mathbf{p}$ and $\mathbf{q}$. It should be noted that while $\mathrm{SID}(\mathbf{s}_i, \mathbf{s}_j)$ is symmetric, $D(\mathbf{s}_i \parallel \mathbf{s}_j)$ is not. This is because $\mathrm{SID}(\mathbf{s}_i, \mathbf{s}_j) = \mathrm{SID}(\mathbf{s}_j, \mathbf{s}_i)$ and $D(\mathbf{s}_i \parallel \mathbf{s}_j) \neq D(\mathbf{s}_j \parallel \mathbf{s}_i)$.

B. Spectral Unmixing, Classification, and Concentration Estimation Algorithms

1) Orthogonal Subspace Projection: OSP is a well-known technique in multispectral/hyperspectral community. It has also been integrated into some commercial products. In this section, the theory is briefly introduced. In the experimental results section, the OSP technique is used as the baseline for comparative studies.

Suppose that there are p targets, $\mathbf{t}_1, \mathbf{t}_2, \ldots, \mathbf{t}_p$. Let $\mathbf{m}_1, \mathbf{m}_2, \ldots, \mathbf{m}_p$ be their corresponding spectral signatures. Suppose L is the number of spectral bands in $\mathbf{m}_j$, where $1 \leq j \leq p$. Let $\mathbf{r}$ denote a linear mixture of $\mathbf{m}_1, \mathbf{m}_2, \ldots, \mathbf{m}_p$ with appropriate abundance fractions specified by $\alpha_1, \alpha_2, \ldots, \alpha_p$, which can be denoted by a $L \times 1$ column vector. Let $\mathbf{M}$ denote the $L \times p$ target spectral signature matrix, depicted by $[\mathbf{m}_1, \mathbf{m}_2, \ldots, \mathbf{m}_p]$. Let $\boldsymbol{\alpha} = [\alpha_1, \alpha_2, \ldots, \alpha_p]^T$ be a $p \times 1$ abundance column vector associated with $\mathbf{r}$, where α_j denotes the abundance fraction of $\mathbf{m}_j$ that is present in the mixture $\mathbf{r}$. The spectral signature of the mixture, $\mathbf{r}$, can be modeled in a linear regression form as

$$\mathbf{r} = \mathbf{M}\boldsymbol{\alpha} + \mathbf{n} \tag{8}$$

where $\mathbf{n}$ is the noise or can be interpreted as a measurement error or a model error. Further, it can be written as

$$\mathbf{r} = \mathbf{d}\alpha_p + \mathbf{U}\gamma + \mathbf{n} \tag{9}$$

where $\mathbf{d} = \mathbf{m}_p$ is denoted as the desired spectral signature $\mathbf{m}_p$ and $\mathbf{U} = [\mathbf{m}_1 \ \mathbf{m}_2 \ \ldots \ \mathbf{m}_{p-1}]$ is the undesired target spectral signature matrix.

An OSP detector denoted by $\delta_{\mathrm{OSP}}(\mathbf{r})$ is given by

$$\delta_{\mathrm{OSP}}(\mathbf{r}) = \mathbf{d}^T P_U^{\perp} \mathbf{r} \tag{10}$$

where $P_U^{\perp} = \mathbf{I}_{L \times L} - \mathbf{U}\mathbf{U}^{\#} = \mathbf{I}_{L \times L} - \mathbf{U}(\mathbf{U}^T\mathbf{U})^{-1}\mathbf{U}^T$.

Based on OSP, a least squares estimator, denoted by $\delta_{\mathrm{LS}}(\mathbf{r})$ which is referred to as *a posteriori* OSP is given by

$$\hat{\alpha}_p = \delta_{\mathrm{LS}}(\mathbf{r}) = \left(\mathbf{d}^T P_U^{\perp} \mathbf{d}\right)^{-1} \delta_{\mathrm{OSP}}(\mathbf{r}). \tag{11}$$

Using (11), the abundance fraction α_p of the desired target signature $\mathbf{m}_p$ in the mixed signature $\mathbf{r}$ is estimated.

2) Nonnegatively Constrained Least Squares Method: The NCLS approach is related to the following optimization problem:

$$\text{Minimize LSE} = (\mathbf{M}\boldsymbol{\alpha} - \mathbf{r})^T (\mathbf{M}\boldsymbol{\alpha} - \mathbf{r}) \text{ subject to } \alpha_j \geq 0 \tag{12}$$

where LSE is the least squares error used as a criterion for optimality, and $\alpha_j \geq 0$ represents the nonnegativity constraint for $1 \leq j \leq p$. In order to use the Lagrange multiplier method, a p-dimensional unknown positive constraint vector

$\mathbf{c} = [c_1, c_2, \ldots, c_p]^T$ with $c_j \geq 0$ is introduced, where $1 \leq j \leq p$. A Lagrangian, $J(\boldsymbol{\alpha})$, by means of $\mathbf{c}$ is formed as

$$J(\boldsymbol{\alpha}) = \left(\frac{1}{2}\right)(\mathbf{M}\boldsymbol{\alpha} - \mathbf{r})^T (\mathbf{M}\boldsymbol{\alpha} - \mathbf{r}) + \boldsymbol{\lambda}^T(\boldsymbol{\alpha} - \mathbf{c}) \tag{13}$$

subject to the constraint $\boldsymbol{\alpha} = \mathbf{c}$. Differentiating $J(\boldsymbol{\alpha})$ with respect to $\boldsymbol{\alpha}$ yields

$$\left.\frac{\partial J(\boldsymbol{\alpha})}{\partial \boldsymbol{\alpha}}\right|_{\hat{\boldsymbol{\alpha}}_{\mathrm{NCLS}}} = 0 = \mathbf{M}^T\mathbf{M}\hat{\boldsymbol{\alpha}}_{\mathrm{NCLS}} - \mathbf{M}^T\mathbf{r} + \boldsymbol{\lambda}. \tag{14}$$

Equation (14) results in the following two iterative equations

$$\hat{\boldsymbol{\alpha}}_{\mathrm{NCLS}} = \left(\mathbf{M}^T\mathbf{M}\right)^{-1} \mathbf{M}^T\mathbf{r} - \left(\mathbf{M}^T\mathbf{M}\right)^{-1} \boldsymbol{\lambda}$$
$$= \hat{\boldsymbol{\alpha}}_{\mathrm{LS}} - \left(\mathbf{M}^T\mathbf{M}\right)^{-1} \boldsymbol{\lambda}, \tag{15}$$

where $\hat{\boldsymbol{\alpha}}_{\mathrm{LS}}$ depicts the least squares estimate of $\boldsymbol{\alpha}$ and is expressed as

$$\hat{\boldsymbol{\alpha}}_{\mathrm{LS}} = \left(\mathbf{M}^T\mathbf{M}\right)^{-1} \mathbf{M}^T\mathbf{r}. \tag{16}$$

Equations (15) and (16) can be used iteratively to solve the optimal solution $\hat{\boldsymbol{\alpha}}_{\mathrm{NCLS}}$ utilizing the Lagrange multiplier vector $\boldsymbol{\lambda} = [\lambda_1, \lambda_2, \ldots, \lambda_p]^T$.

In the NCLS algorithm, the components of the estimate $\hat{\boldsymbol{\alpha}}_{\mathrm{LS}}$ is decomposed into two index sets, which are called active set, R, and passive set, P, respectively. The active set, R, consists of all indexes corresponding to negative (or zero) components. The passive set, P, contains indexes corresponding to positive components in the estimate $\hat{\boldsymbol{\alpha}}_{\mathrm{LS}}$. The algorithm starts with an empty set of P, $P = \varnothing$, assuming that the active set contains all components of $\hat{\boldsymbol{\alpha}}_{\mathrm{LS}}$, $R = \{1, 2, \ldots, p\}$. The sets P and R are then adjusted via iterations using (15) and (16). The final generated passive set depicts the components that are legitimate to be used in the abundance estimation, $\hat{\boldsymbol{\alpha}}_{\mathrm{LS}}$. The NCLS algorithm can be implemented as follows [5]:

```
1. Initialization: Set the passive set P^(k) =
{1,2,...,p}, and active set R^(0) = ∅. Set k = 0.
2. Compute α̂_LS using (16). Let α̂^(k)_NCLS = α̂_LS.
3. At the k-th iteration, if all components
in α̂^(k)_NCLS are positive, the algorithm is termi-
nated; otherwise, continue.
4. Let k ← k + 1.
5. Move all indexes in P^(k-1) that correspond
to negative components of α̂^(k-1)_NCLS to R^(k-1). Let
the resulting index sets be denoted by P^(k) and
R^(k), respectively. Create a new index set S^(k)
and set it to R^(k).
6. Let α̂_R(k) denote the vector consisting of
all components α̂_LS in R^(k).
7. Form a steering matrix Φ^(k)_α by deleting all
rows and columns in the matrix α̂_R(k) specified
by P^(k).
8. Calculate λ^(k)_max = (Φ^(k)_α)^-1 α̂_R(k). If all the
components in λ^(k)_max are negative, go to step 13;
otherwise, continue.
```

9. Calculate $\lambda_{\max}^{(k)} = \max \lambda_j^{(k)}$ and move its index in $R^{(k)}$ to $P^{(k)}$.

10. Form another matrix $\Psi_\lambda^{(k)}$ by deleting every column of $\left(\mathbf{M}^T\mathbf{M}\right)^{-1}$ specified by $P^{(k)}$.

11. Set $\hat{\boldsymbol{\alpha}}_{S(k)} = \hat{\boldsymbol{\alpha}}_{\mathrm{LS}} - \Psi_\lambda^{(k)}\lambda^{(k)}$.

12. If any component of $\hat{\boldsymbol{\alpha}}_{S(k)}$ in $S^{(k)}$ is negative, then move it from $P^{(k)}$ to $R^{(k)}$ and go to step 6.

13. Form another matrix $\Psi_\lambda^{(k)}$ by deleting every column of $\left(\mathbf{M}^T\mathbf{M}\right)^{-1}$ specified by $P^{(k)}$.

14. Set $\hat{\boldsymbol{\alpha}}_{\mathrm{NCLS}}^{(k)} = \hat{\boldsymbol{\alpha}}_{\mathrm{LS}} - \Psi_\lambda^{(k)}\lambda^{(k)}$. Go to step 3.

It may seem that the NCLS method is much more complicated than OSP. However, efficient implementation of NCLS exists, and our simulations indicated that NCLS is actually much faster than the straightforward implementation of OSP. The NCLS method guarantees that the estimated abundance fractions are nonnegative, because there is a constraint about having nonnegative fraction values within the method. On the other hand, since it does not involve a sum-to-one constraint, the sum of the estimated fractions is not equal to 1.

III. EXPERIMENTAL RESULTS

A. SAM and SID As Measures of Spectral Similarity

Three separate datasets were provided by B. Ashman (Army Aberdeen Proving Ground). In this section, the results of applying SAM and SID measures to separate the different agents with respect to the dataset 1 are illustrated. For the other two datasets, details are summarized in [9].

Dataset 1 contains nine agent signatures, eight of which are composed of 880 bands, and one of them consists of 825 bands. Fig. 1 depicts the signature waveforms of the nine agents in dataset 1. With dataset 1, the performance of SAM and SID was investigated with respect to their ability in capturing spectral characteristics.

The similarity values computed by SID regarding the eight signatures (S2-S9) are given in Table I. Table II presents the similarity measures computed by SAM.

In order to determine which of the similarity measures is more effective than the other, the measure of "relative spectral discriminatory power (RSDPW)" [5] was applied to the similarity measure values computed by the SAM and SID methods. Suppose $m(S_i, S_j)$ is the computed similarity measure value between S_i and S_j, where S_i and S_j are the spectral signatures of the two agents. Let $\mathbf{d}$ be the reference agent spectral signature. The RSDPW of $m(S_i, S_j)$ with respect to $\mathbf{d}$ is denoted by $\mathrm{RSDPW}_m(S_i, S_j; \mathbf{d})$ and is mathematically expressed as

$$\mathrm{RSDPW}_m(S_i, S_j; \mathbf{d})$$
$$= \max\left\{\frac{m(S_i, \mathbf{d})}{m(S_j, \mathbf{d})}, \frac{m(S_j, \mathbf{d})}{m(S_i, \mathbf{d})}\right\}. \quad (17)$$

The $\mathrm{RSDPW}_m(S_i, S_j; \mathbf{d})$ value provides a quantitative index of spectral discrimination capability of the similarity measure of interest between two agent signatures, S_i and S_j, relative to $\mathbf{d}$. The higher the $\mathrm{RSDPW}_m(S_i, S_j; \mathbf{d})$ is, the better discriminatory power the $m(S_i, S_j)$ is. The $\mathrm{RSDPW}_m(S_i, S_j; \mathbf{d})$ is equal
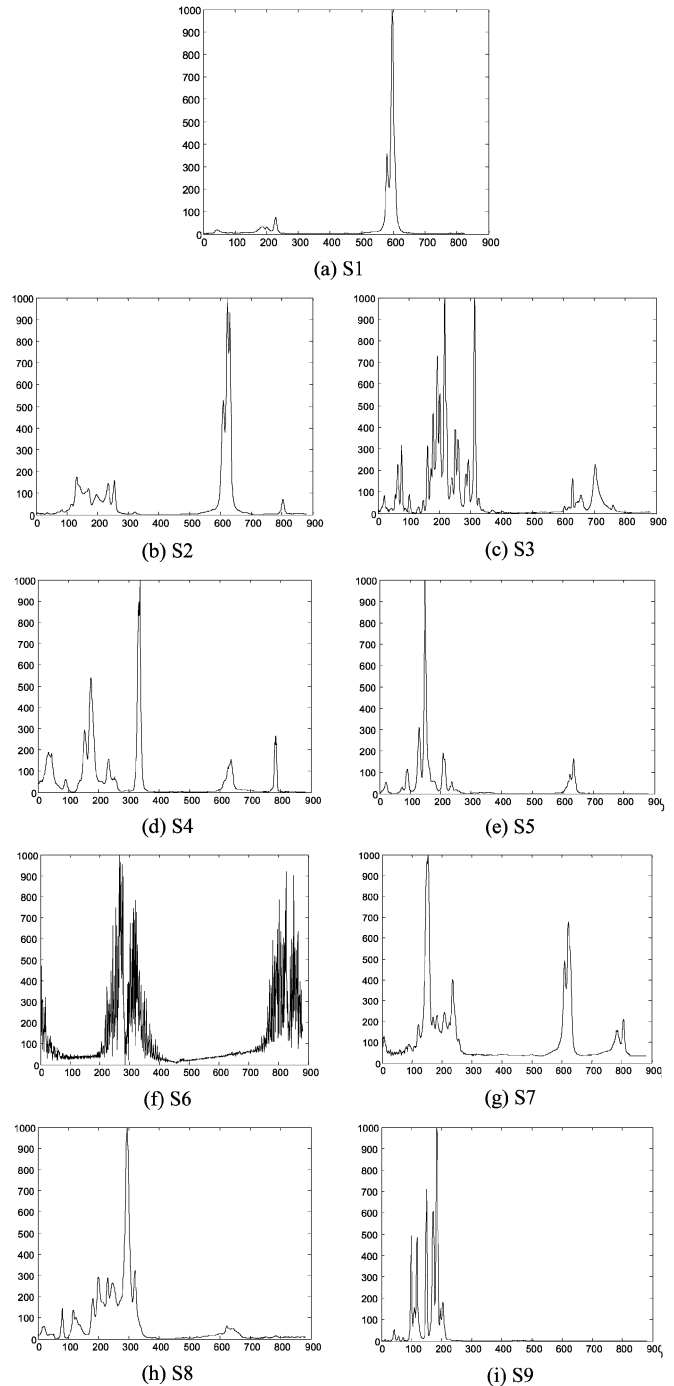

Fig. 1. Agent signatures in dataset 1. S1 band range: 550–3846 (825 bands). S2–S9 band range: 450–3966 (880 bands).

TABLE I
SIMILARITY VALUES PRODUCED BY SID WITH RESPECT TO EIGHT SIGNATURES

	S2	S3	S4	S5	S6	S7	S8	S9
S2	0	3.648	3.514	2.202	4.480	1.069	3.645	6.100
S3		0	3.155	3.949	3.204	2.484	1.676	4.724
S4			0	2.943	3.934	2.185	3.383	4.523
S5				0	5.301	1.314	4.118	3.123
S6					0	2.396	2.495	7.019
S7						0	2.506	3.824
S8							0	5.350
S9								0

to or larger than 1, $\mathrm{RSDPW}_m(S_i, S_j; \mathbf{d}) \geq 1$. It is equal to 1 if and only if $S_i = S_j$.

TABLE II
SIMILARITY VALUES PRODUCED BY SAM WITH RESPECT TO EIGHT SIGNATURES

	S2	S3	S4	S5	S6	S7	S8	S9
S2	0	1.358	1.330	1.266	1.439	0.810	1.387	1.433
S3		0	1.287	1.376	1.223	1.215	1.033	1.288
S4			0	1.267	1.280	1.127	1.328	1.163
S5				0	1.486	0.724	1.425	1.097
S6					0	1.275	1.097	1.514
S7						0	1.266	1.124
S8							0	1.389
S9								0

TABLE III
RSDPW FOR SID WITH REFERENCE SIGNATURE S9

	S3	S4	S5	S6	S7	S8
S3	1.291	1.349	1.953	1.151	1.595	1.140
S4		1.044	1.512	1.486	1.235	1.133
S5			1.448	1.552	1.183	1.183
S6				2.247	1.224	1.713
S7					1.835	1.312
S8						1.399

TABLE IV
RSDPW FOR SAM WITH REFERENCE SIGNATURE S9

	S3	S4	S5	S6	S7	S8
S3	1.112	1.231	1.306	1.056	1.274	1.031
S4		1.107	1.174	1.175	1.146	1.078
S5			1.060	1.301	1.035	1.194
S6				1.380	1.025	1.266
S7					1.346	1.089
S8						1.235

Tables III and IV illustrate the $\text{RSDPW}_m(S_i, S_j; \mathbf{d})$ values, with the assumption that the agent signature, S9, is determined as the reference signature, $\mathbf{d}$. From the results in Tables III and IV, it was observed that in 19 cases out of 21, the $\text{RSDPW}_m(S_i, S_j; \mathbf{d})$ values are higher with SID when compared to SAM. Although it is not illustrated with numerical results, the same trend was observed when another agent (other than S9) was selected as the reference signature. Experiment analyses with the RSDPW measure have demonstrated quantitatively that SID captures spectral characteristics more effectively than SAM. This is because SID is a statistical measure as opposed to SAM, which is considered to be a deterministic measure. Thus, SID measure was used in identifying distinct, slightly distinct, and similar agents that is required to evaluate the performance of the OSP and NCLS methods.

B. OSP and NCLS for Spectral Unmixing, Agent Classification, and Abundance (Concentration) Estimation

1) NIST Datasets Used in the Experiments: Two datasets from the NIST were obtained in this work. In the dataset called "NIST Absorbance May 24, 2004," the total number of agents is 268. The agent signature in this dataset consists of k frequency band points, $k = 88$. In "NIST Transmittance January 19, 2004" dataset, the total number of agents is 225. In this dataset, it was observed that the frequency scaling of some of the agent signatures vary in size and frequency resolution. In order to overcome and include the same frequency band regions in the agent signatures, the start and end points of the frequency bands were selected as 1000 and 3000, respectively. The frequency band resolution was set to 5. Thus, a total number of 401 frequency

TABLE V
AGENTS USED IN EXPERIMENT 1

Agent no	Agent name	Agent no	Agent name
1	2-chloroethylmethylsulfide	11	Acetylacetone
2	Diethyl ethylphosphonate	12	3-amino-1-propanol
3	Ethanol	13	Aniline
4	Freon 114	14	Benzoic acid
5	n-butyl bromide	15	Benzyl acetate
6	Bis-2-ethyl-1-hexyl phosphonate	16	Bis-hydrogen phosphite
7	Benzyl benzoate	17	2-Bromoethanol
8	Dibenzyl Ether	18	1-Butoxyethoxy-2-propanol
9	Piperidine	19	1-Butoxy-2-propanol
10	3-Hydroxy-2-butanone	20	n-Butyl benzoate

(a) IR spectrum of *Ethanol*

(b) IR spectrum of *3-Hydroxy-2-butanone*

(c) IR spectrum of *1-Butoxyethoxy-2-propanol*

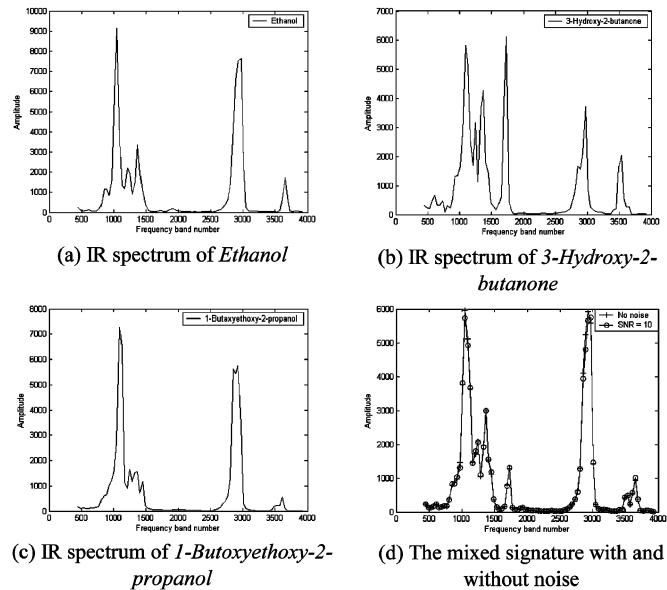(d) The mixed signature with and without noise

Fig. 2. IR spectrums of the mixture components and the mixed signature with and without noise.

band points were obtained from the corresponding agent signatures in the "NIST Transmittance January 19, 2004" dataset, $k = 401$.

2) Performance of OSP:

Experiment 1: Concentration estimation of an artificially degraded mixed signature with 20 agents in the database selected from the NIST Absorbance May 24, 2004 dataset (agent signatures have 88 frequency band points)

In Experiment 1, a mixed-agent signature t was generated among a total of 20 agents in the signature database, Δ. Thus, Δ consists of 20 agents, $\Delta = \{\mathbf{s}_1, \ldots, \mathbf{s}_{20}\}$. The 20 agents were selected from the NIST Absorbance May 24, 2004 dataset. The agents in Δ are depicted in Table V.

The number of frequency band points in each of the agent signature is 88. Three agents $\mathbf{s}_3$, $\mathbf{s}_{10}$, and $\mathbf{s}_{18}$ were included in the mixture, t, with different abundance fractions. The agent $\mathbf{s}_3$ stands for *Ethanol*; $\mathbf{s}_{10}$ stands for *3-Hydroxy-2-butanone*; and $\mathbf{s}_{18}$ stands for *1-Butoxyethoxy-2-propanol*. The abundance fractions for $\mathbf{s}_3$, $\mathbf{s}_{10}$, and $\mathbf{s}_{18}$ were selected as 0.50, 0.20, and 0.30, respectively. In addition, white Gaussian noise was added to t such that the signal-to-noise ratio (SNR) became 10, 50, and
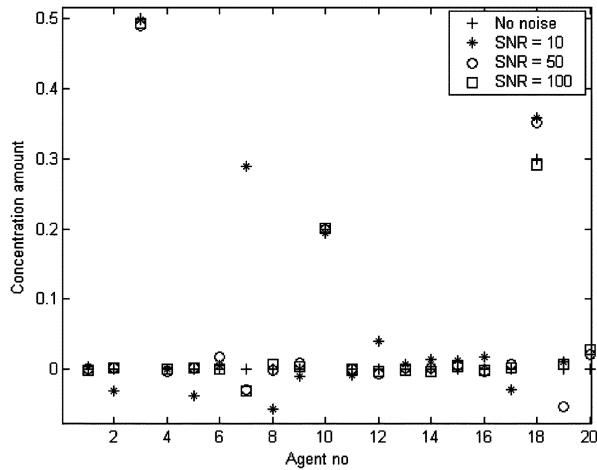
Fig. 3.	Estimated abundance fraction coefficients of the mixture.

Fig. 4.	Signature waveform for Freon.

100, respectively. The IR spectra of the components of the mixture and the mixed signature without noise and with a SNR value of 10 are depicted in Fig. 2. The SNR is defined as the ratio of 50% reflectance to noise standard deviation. Since SNR is defined in terms of a ratio, no unit is included after the statement of SNR values in the content of this paper.

The OSP method was applied to the generated target mixed signature, t. Three different SNR values (10, 50, and 100) were investigated. Fig. 3 depicts the estimated abundance fractions with noise-free and three SNR values. It was observed that the OSP approach can estimate the abundance fractions of the agents in the generated target mixed signature with different SNR values. On the other hand, the accuracy of the estimated fractions dropped in accordance with the amount of noise embedded in the mixture signature. It was seen that there are inaccurate abundance fraction estimates for agents, which are not included in t, as the amount of noise is increased.

Experiment 2: Concentration estimation of an artificially degraded mixed signature with distinct database (93 agents in the database) selected from the NIST Transmittance January 19, 2004 dataset, (agent signatures have 401 frequency band points) using OSP method

In Experiment 2, the NIST Transmittance January 19, 2004 dataset was used. A preprocessing, which included interpolation, start and end frequency band points determination, was applied to this dataset in order to fix the number of frequency band points and frequency resolution. In order to demonstrate to the readers how the agent signatures look like, the signature waveform of Freon is depicted in Fig. 4.

In this experiment, the performance of the OSP method was evaluated with a database that consisted of 93 distinct agents. This database is called *distinct database*. The determination of the distinctness between the agents was found by using the SID similarity measure. In the *distinct database*, the minimum value for the SID measure between any two agents was found to be 0.0514. Please note that the lower the SID measures, the more similar the two agents are. The mixed-agent signature was composed of five agents in the distinct database. These agents were {**s2** (Freon 113), **s6** (Benzoic acid), **s46** (2-Chlorophenol), **s69** (Formic acid), **s85** (Thymine)}. The abundance fractions of
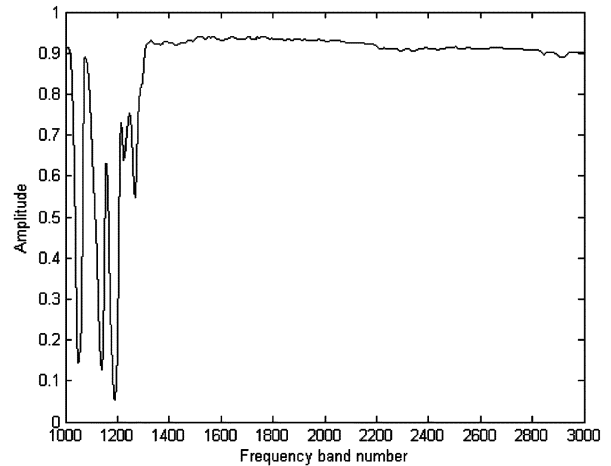
these five agents that formed the mixture were selected as 1.0, 1.5, 2.0, 2.5, and 0.5, respectively. An SNR value of 20 was applied to the generated mixture. Fig. 5(a) depicts the actual and the estimated abundance fractions in the mixed-agent signature by the OSP method. Fig. 5(b) introduces the same information in another presentation form. In this form, the points will be located on a diagonal line if the abundance fractions are correctly estimated. The performance of OSP was not satisfactory because there were inaccurate fraction estimations as well as some large negative estimates for those agents with zero fractions.

Two additional experiments were conducted with the OSP method using two other agent databases. One of the two databases consisted of 156 agents. In this database, there were a number of agents that were slightly distinct. This database is called *slightly distinct database*. The minimum value for the SID measure between any two agents in the *slightly distinct database* was found to be 0.0201. The other database consisted of 197 agents, and in this database, there were a number of agents, which had similar signature waveforms. This database is named *similar database*. The minimum value for the SID measure between any two agents in the *similar database* was found to be 0.0051. From Experiment 2 and the two additional experiments, it was seen that as the number of agents is increased and there are similar agents in the database, the performance of the OSP method drops significantly. Please refer to [9] for the results of these additional experiments.

The simulation results in the experiments with the OSP method indicated that the OSP method can accurately estimate the abundance fractions of the agents that form the mixed-agent signature, if the agent signatures in the database are distinct. The signatures in the database should not be same or very close to each other; otherwise, matrix singularity causes inaccurate concentration estimates. The amount of noise embedded in the mixed signature also affects the performance of the OSP, which has been demonstrated in the experiments.

3) Performance of NCLS:

Experiment 3: Concentration estimation of an artificially degraded mixed signature with distinct database (93 agents in the database) selected from the NIST Transmittance January 19, 2004 dataset, (agent signatures have 401 frequency band points) using NCLS method
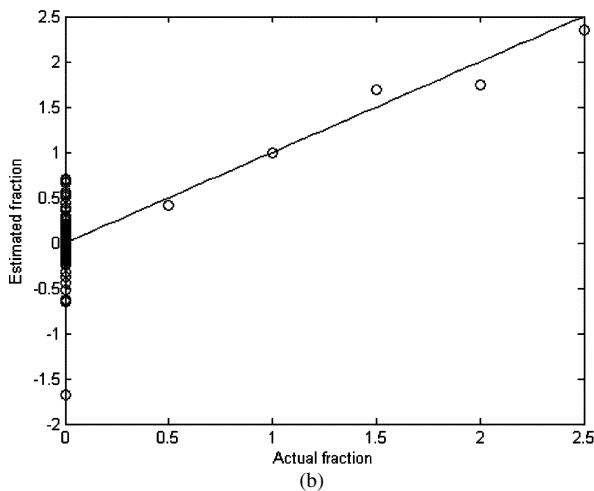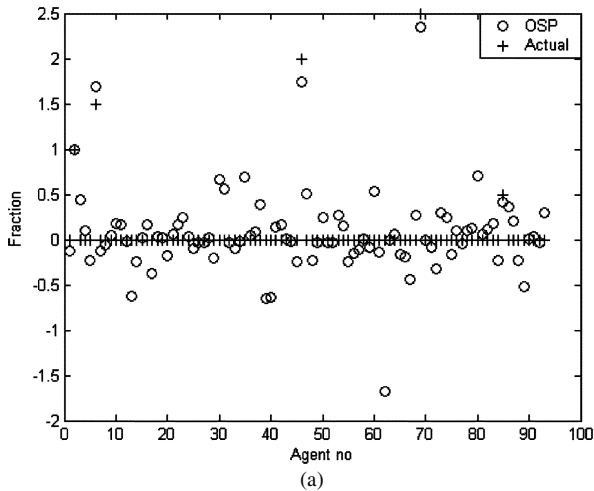
Fig. 5.   Actual and estimated abundance fractions by the OSP with the distinct database.
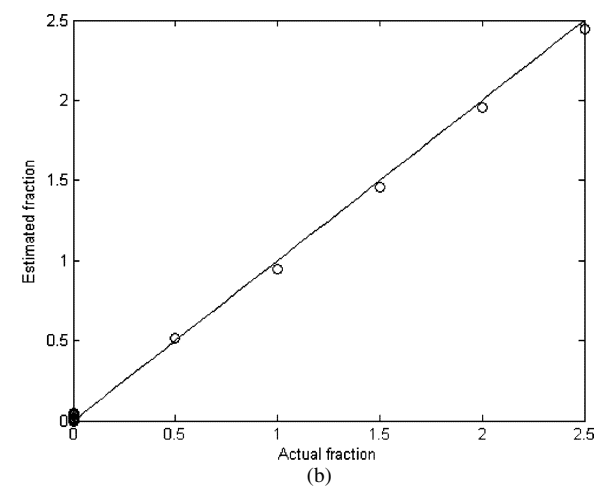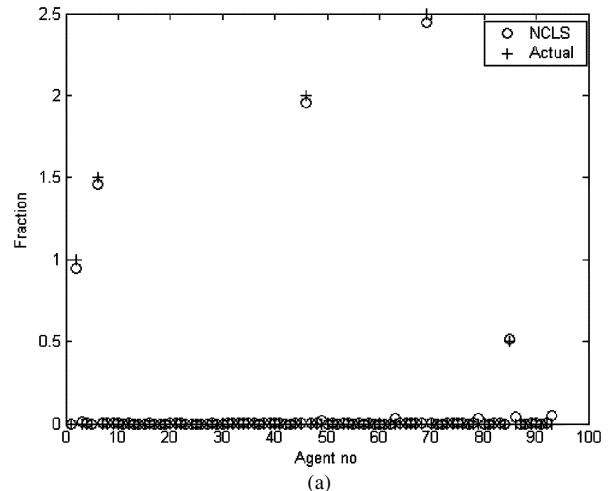

Fig. 6.   Actual and estimated abundance fractions by NCLS with the *distinct database*.

In Experiment 3, the performance of a relatively new technique, NCLS [5], was investigated. The performance of the NCLS method was evaluated using 93 agents in the distinct database. The mixed-agent signature was composed of five agents in the distinct database, which were {**s2** (Freon 113), **s6** (Benzoic acid), **s46** (2-Chlorophenol), **s69** (Formic acid), **s85** (Thymine)}. The corresponding abundance fractions of the agents in the mixed signature were selected as 1.0, 1.5, 2.0, 2.5, and 0.5, respectively. The applied SNR value to the mixed-agent signature was 20. Fig. 6 depicts the actual and estimated abundance fractions in the mixed-agent signature using the two presentation forms. Compared to Fig. 5, which used OSP for estimation, the NCLS results in Fig. 6 were much more accurate and also there were no negative concentration estimates.

Experiment 4: Concentration estimation of an artificially degraded mixed signature with slightly distinct database (156 agents in the database) selected from the NIST Transmittance January 19, 2004 dataset, (agent signatures have 401 frequency band points) using NCLS method

In Experiment 4, the performance of the NCLS method was evaluated with the slightly distinct database that had 156 agents. The same agent mixture, which has been used in Experiments 3

and 4 with SNR value of 20, was formed, {**s2** (Freon 113), **s6** (Benzoic acid), **s46** (2-Chlorophenol), **s69** (Formic acid), **s85** (Thymine)} with abundance fractions 1.0, 1.5, 2.0, 2.5, and 0.5. Fig. 7 depicts the actual and estimated abundance fractions in the mixture. The results are still very accurate.

Experiment 5: Concentration estimation of an artificially degraded mixed signature with similar database (197 agents in the database) selected from the NIST Transmittance January 19, 2004 dataset, (agent signatures have 401 frequency band points) using NCLS method

In Experiment 5, the performance of the NCLS method was evaluated with the *similar database* that had 197 agents. The same mixture, which has been used in Experiment 2–4, was formed with SNR value of 20. Fig. 8 depicts the actual and estimated abundance fractions in the mixture. The results are reasonably good.

4) Comparison of the OSP and NCLS Methods:

Accuracy of the Concentration Estimates: In the light of these experimental results, it was observed that the performance of the OSP method degrades as the number of agents in the database is increased by the addition of new agents that have similar signature waveforms. On the other hand, the NCLS method
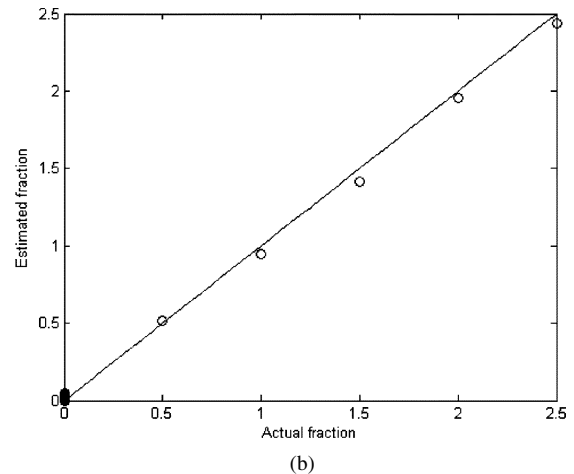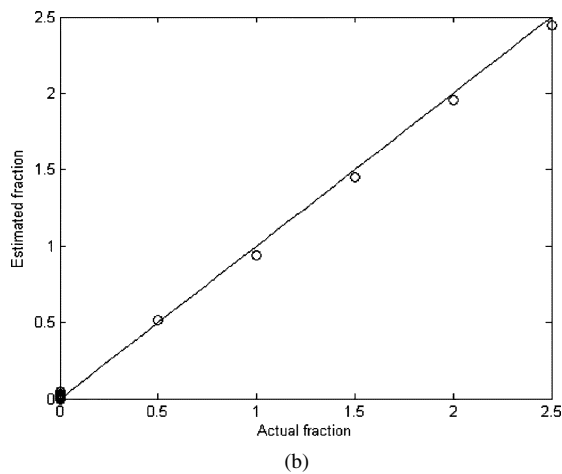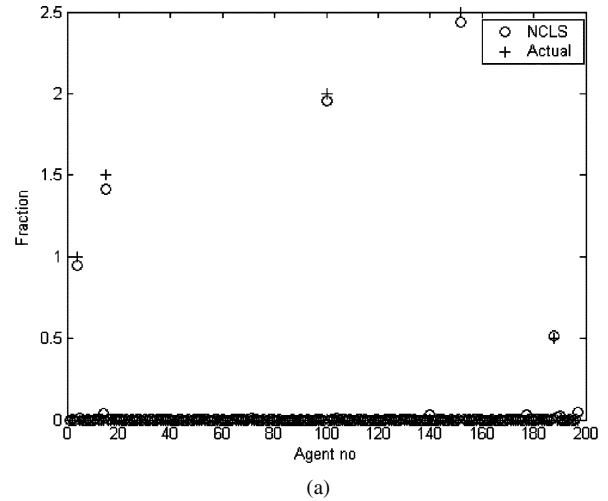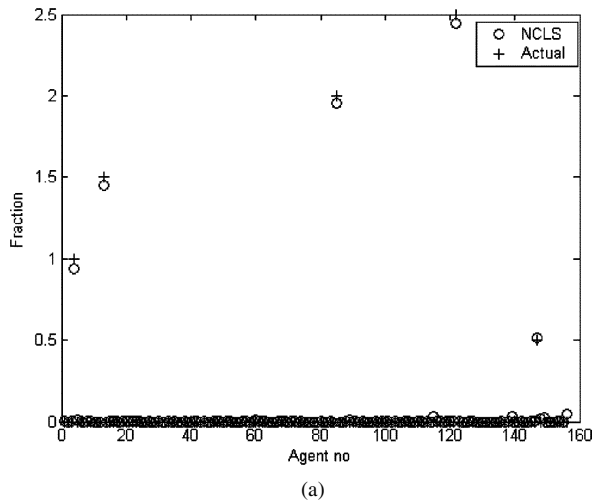
(a)

(b)

Fig. 7. Actual and estimated abundance fractions by NCLS with the *slightly distinct database*.

(a)

(b)

Fig. 8. Actual and estimated abundance fractions by the NCLS with the *similar database*.

(Figs. 6–8) outperforms the performance of the OSP method. It is worth mentioning that no negative abundance fractions were observed with the NCLS method. Fig. 9 depicts the sum of absolute fraction errors with respect to the three agent databases (distinct, slightly distinct, and similar). The sum of absolute fraction errors is mathematically expressed in (17). It is seen from Fig. 9 that the error values in NCLS is much smaller than OSP for all the three databases

$$\text{Sum of absolute fraction error} = \sum_{i=1}^{N} \left| y_i^{\text{est}} - y_i^{\text{act}} \right|$$

N : Number of agents in the mixture

y_i^{act} : Fraction estimate of the ith agent in the mixture

y_i^{est} : Actual fraction of the ith agent in the mixture. (18)

Performance Under Different Noise Levels Using the NIST Transmittance January 19, 2004 Dataset: The performance of the NCLS method under different noise levels was evaluated using the *distinct database* of 93 agents. In this experiment, 20 mixtures were generated randomly, in which each mixture was composed of five agents. The abundance fractions of the agents in the mixtures were randomly generated between 0 and 1. A number of SNR values have been experimented (SNR = 20, 30, 40, 50, 100, and no noise). Fig. 10 depicts the average
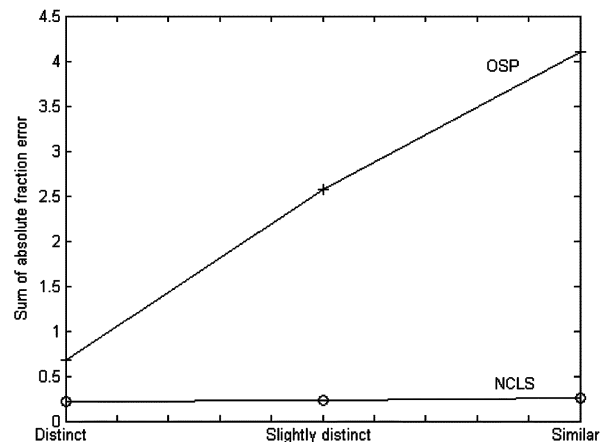

Fig. 9. Sum of absolute fraction errors versus used databases for the OSP and NCLS methods.

of the sum of absolute fraction errors for the randomly generated mixtures under different SNR. From Fig. 10, it is seen that NCLS shows significantly smaller error, as compared to OSP.

5) Performance of the NCLS Method With Ten Agents in a Single Mixture Under Different Noise Levels (NIST Transmittance January 19, 2004): In this analysis, the number of agents that form the mixed-agent signature was increased from 5 to 10. The performance of the NCLS method was evaluated using
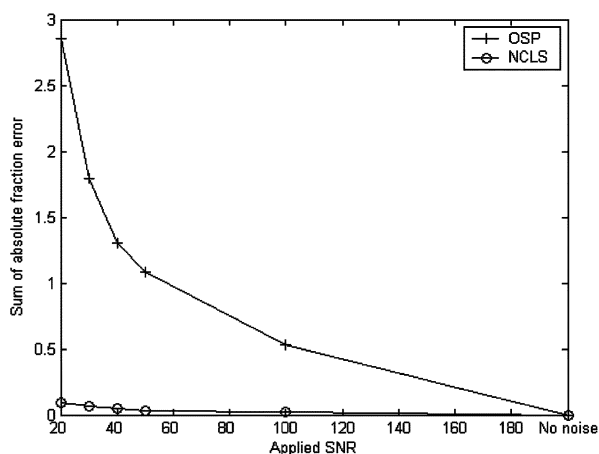
Fig. 10. Average of the sum of absolute fraction errors for the randomly generated mixtures under different SNR.
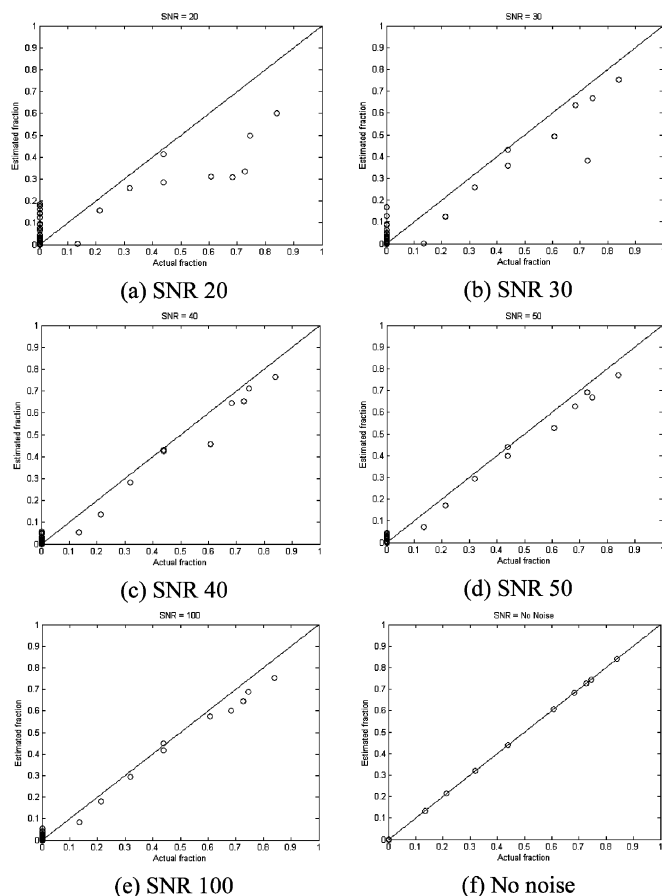

Fig. 11. Actual and estimated abundance fractions under different noise levels with a mixture of ten agents. Signature database has 197 agents.

the similar agent database that had 197 agents. The abundance fractions of the agents in the mixtures were randomly generated between 0 and 1. A number of SNR values have been experimented (SNR = 20, 30, 40, 50, 100, and no noise). Fig. 11 depicts the actual and estimated abundance fraction estimates with respect to six SNR levels. Regarding the plots in Fig. 11, it can be seen that as the noise amount drops, the diagonal shape becomes more distinct indicating that the estimation accuracy improves.

It was clearly demonstrated from the experiments and the performance analyses that the NCLS method performs effi-

ciently and yields accurate abundance fraction estimates when the number of agents that form the agent mixture signature is increased in the presence of noise. In further experiments, the number of agents in the formed mixture was increased up to 20, and still considerably acceptable abundance fraction estimates were obtained. For results and details regarding these experiments, please refer to [9].

The experiments and the corresponding analyses indicated that the NCLS method is a promising method in chemical and biological agent detection and concentration estimation. The NCLS method does not generate negative fractions. Yet, in the case of adding similar agents to the database and increasing the number of agents in the agent mixture signature, the accuracy of the NCLS method in agent detection and abundance fraction estimation does not degrade significantly and still provides reasonable results. Thus, for detecting chemical and biological agents, which are in the form of mixtures, and estimating their abundance fractions, NCLS was found to provide significant opportunities in letting to respond with fast reaction times and in decreasing the potential damage to minimal levels. The future works of this research include using real mixed data and taking into account different noise levels. We are in contact with the U.S. Army and NIST to obtain real mixture datasets, which are collected from controlled experiments and from the field. Once having these real datasets, the second part of our research will be to apply the developed algorithms on these datasets.

IV. CONCLUSION

In a chemical and biological agent attack, it is possible that the chemical and biological agents can be composed in the form of mixture clouds in order to make the existing agent detection systems, which are specific to single agents, useless. The detection of agents in the form of mixtures is a more challenging problem than detecting the agents alone. In this research, the use of spectral unmixing techniques (OSP and NCLS), which are extensively used in hyperspectral imaging, were investigated for chemical biological agent detection and concentration estimation. Experimental datasets have been provided by the U.S. Army and NIST. These datasets included chemical and biological agent signatures, which were collected by the infrared spectrum technique. The experimental results and the corresponding analyses indicated that NCLS is a very promising method in detecting chemical and biological agents, which are composed in the form of mixture clouds. In addition to correctly identifying the agents that form the mixture, the NCLS method also provided accurate abundance fraction estimates even if the agent signatures in the related database had similar waveforms. Since NCLS is an optimization technique based on a nonnegative constraint, none of the estimated abundance fraction estimates are negative, which is thus more consistent with a real-life scenario. The experimental and analysis works in this paper have been done by using a graphical user interface, which was specifically developed for this research.

REFERENCES

[1] H. H. Hill and S. J. Martin, "Conventional analytical methods for chemical warfare agents," *Pure Appl. Chem.*, vol. 74, no. 12, pp. 2281–2291, 2002.
[2] G. M. Murray and G. E. Southard, "Sensors for chemical weapons detection," *IEEE Instrum. Meas. Mag.*, no. 4, pp. 12–21, Dec. 2002.
[3] D. C. Meier et al., "Chemical warfare agent detection using MEMS-compatible microsensor arrays," *IEEE Sensors J.*, vol. 5, no. 4, pp. 712–725, Aug. 2005.
[4] R. R. Bousquet et al., "Trends in microwave spectroscopy for the detection of chemical agents," *IEEE Sensors J.*, vol. 5, no. 4, pp. 656–664, Aug. 2005.
[5] C. Chang, *Hyperspectral Imaging*. Dordrecht, The Netherlands: Kluwer, 2003.
[6] ——, "Orthogonal subspace projection (OSP) revisited: A comprehensive study and analysis," *IEEE Trans. Geosci. Remote Sens.*, vol. 43, no. 3, pp. 502–518, Mar. 2005.
[7] Q. Du and C.-I Chang, "Linear mixture analysis-based compression for hyperspectral image analysis," *IEEE Trans. Geosci. Remote Sens.*, vol. 42, no. 4, pp. 875–891, Apr. 2004.
[8] Q. Du, H. Ren, and C.-I Chang, "A comparative study for orthogonal subspace projection and constrained energy minimization," *IEEE Trans. Geosci. Remote Sens.*, vol. 41, no. 6, pp. 1525–1529, Jun. 2003.
[9] C. Kwan et al., "A novel approach for spectral unmixing and classification of chemical and biological agents.," U.S. Air Force, Wright Patterson AFB, MI, Phase 1 Final Report for the Air ForceWright Patterson Lab under Contract FA8650-04-M-1606, 2004.
[10] C.-I Chang and D. C. Heinz, "Constrained subpixel target detection for remotely sensed imagery," *IEEE Trans. Geosci. mote Sens.*, vol. 38, no. 3, pp. 1144–1159, May 2000.
[11] S. Kullback, *Information Theory and Statistics*. New York: Wiley, 1959.

Bulent Ayhan (S'01) received the B.S. and M.S. degrees in electrical and electronics engineering from Bogazici University, Istanbul, Turkey, in 1998 and 2000 respectively. He is currently pursuing the Ph.D. degree in electrical and computer engineering at North Carolina State University, Raleigh.

His research interests include condition monitoring, fault detection, and diagnostics.

Mr. Ayhan is a member of Phi Kappa Phi.

Genshe Chen received the B.S. and M.S. degrees in electrical engineering and the Ph.D. degree in aerospace engineering from Northwestern Polytechnical University, Xian, China, in 1989, 1991, and 1994, respectively.

He did postdoctoral work at the Beijing University of Aeronautics and Astronautics and Wright State University from 1994 to 1997. He worked at the Institute of Flight Guidance and Control of the Technical University of Braunshweig (Germany) as an Alexander von Humboldt Research Fellow and at the Flight Division of National Aerospace Laboratory of Japan as an STA Fellow from 1997 to 2001. He was a Postdoctoral Research Associate at the Department of Electrical and Computer Engineering, The Ohio State University, from 2002 to 2004. Since February 2004, he has been with Intelligent Automation, Inc. (IAI), Rockville, MD, where he is a Senior Research Scientist. At IAI, he is involved in several projects such as speech recognition with fusion of video and audio data, smart flow system, and biological and chemical agent detection. He has been the technical lead on several projects such as maneuvering target detection and tracking with radar range rate information, game-theoretic cooperative path and mission planning for multiple aerospace vehicles, stochastic differential pursuit-evasion game with multiple players, and a game-theoretic approach to threat prediction and situation awareness. His research interests include guidance and control of aerospace vehicles; GPS/INS/camera-integrated navigation systems; target detection, identification, and tracking; data fusion; cooperative control and optimization; computational intelligence and data mining; hybrid system theory and Markov chains; signal processing and computer vision; cooperative and noncooperative game theory; and GIS.

Chiman Kwan (S'85–M'93–SM'98) received the degree in electronics with honors from the Chinese University of Hong Kong, Hong Kong, and M.S. and Ph.D. degrees in electrical engineering from the University of Texas, Arlington, in 1988, 1989, and 1993, respectively.

From April 1991 to February 1994, he worked in the Beam Instrumentation Department, Superconducting Super Collider (SSC) Laboratory, Dallas, TX, where he was heavily involved in the modeling, simulation, and design of modern digital controllers and signal processing algorithms for the beam control and synchronization system. He received an invention award for his work at SSC. Between March 1994 and June 1995, he joined the Automation and Robotics Research Institute, Fort Worth, TX, where he applied intelligent control methods such as neural networks and fuzzy logic to the control of power systems, robots, and motors. Since July 1995, he has been with Intelligent Automation, Inc., Rockville, MD. He has served as Principal Investigator/Program Manager for more than 65 different projects, with total funding exceeding U.S. $20 million, such as modeling and control of advanced machine tools, digital control of high-precision electron microscopes, enhancement of microscope images, and adaptive antenna arrays for beamforming, automatic target recognition of FLIR and SAR images, fast flow control in communication networks, vibration management of gun pointing system, health monitoring of electromechanical systems, high-speed piezoelectric actuator control, fault-tolerant missile control, speech enhancement, and underwater vehicle control. One of the projects related to Space Shuttle Auxiliary Power Unit monitoring received a NASA Space Act Award. Currently, he is the Vice President, leading research and development efforts in signal/image processing, and controls. His primary research areas include fault detection and isolation, robust and adaptive control methods, signal and image processing, communications, neural networks, and pattern recognition applications. He has published more than 35 papers in archival journals and has had 90 additional papers published in major conference proceedings.

Dr. Kwan is listed in the New Millennium edition of *Who's Who in Science and Engineering* and is a member of Tau Beta Pi.

Jing Wang (S'03) received the B.S. degree in electrical engineering and M.S. degree in computer engineering from Beijing University of Post and Telecommunications (BUPT), Beijing, China, and the M.S. degree in electrical engineering from University of Maryland Baltimore County (UMBC), Baltimore, in 1998, 2001, and 2005, respectively. She is currently pursuing the Ph.D. degree at UMBC.

Her research interests include multispectral/hyperspectral image processing, signal detection and estimation, and pattern recognition.

Baohong Ji (S'05) received the B.S. and M.S. degrees in computer science from Jilin University of Technology, Jilin, China, in 1993 and 1996, respectively. She is currently pursuing the Ph.D. degree at the University of Maryland Baltimore County, Baltimore.

From 1997 to 2000, she served as a Lecturer in Jilin University of Technology. Her research interests include remote sensing, image processing, data compression, and pattern recognition.

Chein-I Chang (S'81–M'87–SM'92) received the B.S. degree from Soochow University, Taipei, Taiwan, R.O.C., in 1973, the M.S. degree from the Institute of Mathematics, National Tsing Hua University, Hsinchu, Taiwan, in 1975, and the M.A. degree from the State University of New York, Stony Brook, in 1977, all in mathematics. He received the M.S. and M.S.E.E. degrees from the University of Illinois at Urbana-Champaign in 1982 and the Ph.D. degree in electrical engineering from the University of Maryland, College Park, in 1987.

He has been with the University of Maryland Baltimore County (UMBC), Baltimore, since 1987, as a Visiting Assistant Professor from January 1987 to August 1987, Assistant Professor from 1987 to 1993, Associate Professor from 1993 to 2001, and Professor in the Department of Computer Science and Electrical Engineering since 2001. He was a Visiting Research Specialist in the Institute of Information Engineering at the National Cheng Kung University, Tainan, Taiwan, from 1994 to 1995. He has three patents on automatic pattern recognition and several pending patents on image processing techniques for hyperspectral imaging and detection of microcalcifications. His research interests include multispectral/hyperspectral image processing, automatic target recognition, medical imaging, information theory and coding, signal detection and estimation, and neural networks. He is the author of a book *Hyperspectral Imaging: Techniques for Spectral Detection and Classification* (Kluwer). He is on the editorial board and was the Guest Editor of a special issue on telemedicine and applications of the *Journal of High Speed Networks*.

Dr. Chang received a National Research Council Senior Research Associateship Award from 2002 to 2003 at the U.S. Army Soldier and Biological Chemical Command, Edgewood Chemical and Biological Center, Aberdeen Proving Ground, MD. He is an Associate Editor in the area of hyperspectral signal processing for the IEEE TRANSACTIONS ON GEOSCIENCE AND REMOTE SENSING. He is a Fellow of SPIE and a member of Phi Kappa Phi and Eta Kappa Nu.